Research article

Ryan Cardman*, Luís F. Gonçalves, Rachel E. Sapiro, Georg Raithel and David A. Anderson*

Atomic 2D electric field imaging of a Yagi–Uda antenna near-field using a portable Rydberg-atom probe and measurement instrument

https://doi.org/10.1515/aot-2020-0029
Received June 17, 2020; accepted September 5, 2020;
published online October 5, 2020

Abstract: We present electric field measurements and imaging of a Yagi–Uda antenna near-field using a Rydberg atom–based radio frequency electric field measurement instrument. The instrument uses electromagnetically induced transparency with Rydberg states of cesium atoms in a room-temperature vapor and off-resonant RF-field–induced Rydberg-level shifts for optical SI-traceable measurements of RF electric fields over a wide amplitude and frequency range. The electric field along the antenna boresight is measured using the atomic probe at a spatial resolution of $\lambda_{RF}/2$ with electric field measurement uncertainties below 5.5%, an improvement to RF measurement uncertainties provided by existing antenna standards.

Keywords: antenna measurement; coherent optical effects; metrology; quantum detectors; remote sensing and sensors; Rydberg states.

1 Introduction

Measurement and imaging of radio frequency (RF) electric fields emitted by radiating electronic systems is critical to RF systems development and engineering, RF metrology and calibration, and electromagnetic testing in industries spanning from aerospace and defense to wireless communications and consumer electronics. To date, antennas constitute a critical interface between freely propagating RF fields and electronics units, affecting transmission and reception of RF fields [1, 2]. Antenna technology involves the coupling between electromagnetic fields and RF currents in physical conductors with specific geometric and material properties [3], bringing about limitations in certain fundamental performance metrics, such as frequency coverage and measurement accuracy [4]. The practical utility of antennas is further hampered by their large sizes and metal composition, which preclude RF field measurements at small spatial scales and in proximity to other conductive structures [5].

Narrow-line optical spectroscopy of Rydberg states of atoms in room-temperature vapors has come to prominence as a novel quantum sensor technology platform for optical measurements of RF electric fields that removes many of these antenna limitations. Rydberg atom–based detectors use the physics of Rydberg atoms [6], which are atoms with valence electrons in highly excited energy levels, and electromagnetically induced transparency (EIT) [7–9] for optical probing of Rydberg-atom energy levels. In the presence of RF fields, these energy levels are shifted and split, and these shifts and splittings can be modeled via the AC Stark effect and Autler–Townes couplings [7, 10] in addition to Floquet methods for RF field measurement [11, 12]. The enhanced electric field sensitivity of Rydberg atoms combined with EIT in room-temperature vapors [13] has afforded the development of electrometry using miniature alkali vapor cells [11, 12, 14–18]. A Rydberg atom–based field detector, consisting of an alkali vapor of Rydberg atoms contained within dielectric cells, can be realized on a much smaller size scale than the RF wavelength of interest, allowing high-resolution, subwavelength, near-field imaging of radiation patterns [19]. In addition, owing to the absence of metal parts, these field sensors do not mutually couple with the transmitter and therefore do not distort the measured radiation pattern as conventional antennas or resonators do. Mutual coupling occurs when the RF current induced within the antenna by the incident radiation reradiates into free space and toward the transmitter [20]. However, a dilute gas

***Corresponding authors: Ryan Cardman and David A. Anderson**, Rydberg Technologies Inc., Ann Arbor, MI, USA; and Department of Physics, University of Michigan, Ann Arbor, MI, USA, E-mail: rcardman@umich.edu (R. Cardman), dave@rydbergtechnologies.com (D.A. Anderson)
Luís F. Gonçalves and Rachel E. Sapiro, Rydberg Technologies Inc., Ann Arbor, MI, USA
Georg Raithel, Rydberg Technologies Inc., Ann Arbor, MI, USA; Department of Physics, University of Michigan, Ann Arbor, MI, USA

of Rydberg atoms cannot strongly reradiate the incident fields.

Modern tools used in antenna design across the electromagnetic spectrum are commonly based on field measurement in the near-field and near-field–to–far-field transformation [21, 22]. It is therefore of considerable interest to scale down the size and electromagnetic cross section of RF measurement probes for high-resolution accurate electric field measurement in the near-field. Rydberg atom–based RF field sensors address this need in addition to providing direct SI-traceable measurement and high measurement accuracy.

In this work, we demonstrate subwavelength electric field measurement and imaging of an RF Yagi–Uda antenna near-field using a portable Rydberg Field Probe (RFP) and Measurement System (RFMS), the first standalone instrument of its kind using optical Rydberg EIT spectroscopy in an atomic vapor for SI-traceable RF measurement [23]. This instrument differs from other approaches in that this device is an autonomous system that encompasses a fully characterized probe head and a control/laser package that implements absolute, high-precision field and field uncertainty measurements [23]. The probe head is portable with a minimal RF footprint; unlike table-top Rydberg atom experiments, the low-profile and characterized probe can be accurately positioned and oriented relative to a device under test (DUT). It is this feature, in particular, that allows for accurate measurement and mapping of an antenna's emission pattern.

Although Yagi–Uda antennas have been scaled to sub-μm sizes [24] for the efficient coupling of laser modes into plasmonic integrated circuits and characterized in the near-field [24, 25] at optical infrared frequencies, direct measurement and imaging of the near-field of an RF Yagi–Uda antenna using an atomic probe has not been demonstrated to date. Although there exist conventional antennas and non–atom-based probes for the direct and indirect measurement of RF electric fields in the transmitter's reactive and radiating near-field, allowing for characterizations of RF Yagi–Uda antennas [26], they remain subject to the practical and fundamental limitations described. Here, we use the atom-based probe to perform SI-traceable measurements and image the electric field radiation pattern in the near-field of a Yagi–Uda antenna transmitting at 2.5 GHz.

An image of the 2.5 GHz electric field is realized by rastering the atomic probe over a 1.9 × 0.5 m area in the near-field of the Yagi–Uda antenna and along its boresight at a $\lambda_{RF}/2$ spatial resolution with total measurement uncertainties $\lesssim$5.5%, equivalent to state-of-the-art antenna standards [4]. We also describe the theory and application of off-resonant, RF-field level shifts in alkali Rydberg atoms implemented in the probe for measurement of RF fields over a wide amplitude and frequency range, suitable for practical applications in metrology and broader RF testing and measurement with Rydberg atom–based detectors.

2 Theory of Rydberg atom–based field sensing

Rydberg states are extremely sensitive to RF fields over a wide range of frequencies. The effects of RF fields on Rydberg states can be optically detected using EIT spectroscopy. In the present implementation, a weak probe laser resonant with the cesium (Cs) D2 line ($6S_{1/2}$ to $6P_{3/2}$ electric-dipole transition) [27] passes through the atomic-detection region in a Cs vapor cell and onto a photodiode. In this configuration, one observes a reduction in the laser's intensity due to absorption from the atoms. When a second laser field, known as the coupler, resonantly drives an electric-dipole transition between the intermediate ($6P_{3/2}$) state and another state, which is a $nS_{1/2}$ Rydberg state in the present case, the atoms typically reside in a quantum superposition of the $6S_{1/2}$ and the $nS_{1/2}$ state. The excitation amplitude into the intermediate state $6P_{3/2}$ state then exhibits destructive interference, resulting in a transparency of the probe laser through the atomic medium known as EIT [7–9]. The probe laser's transmission as a function of the coupler laser frequency features a sharp spectroscopic EIT peak where the coupler laser is resonant with the transition frequency from the intermediate to the Rydberg state.

The exact spectroscopic location of the Rydberg-EIT peak allows one to accurately monitor RF-induced shifts of the Rydberg state's energy level. This includes shifts caused by external RF fields, the type of shift relevant in the present work. The optically measured Rydberg line shift allows one to measure the RF electric field amplitude that is directly SI-traceable to fundamental constants and invariable atomic parameters. Here we concentrate on Rydberg AC energy level shifts as a field indicator. In RF fields, $\mathbf{E}(t) = \hat{\epsilon} E_0 \cos(\omega_{RF} t)$ with weak to moderate electric field amplitudes E_0, the Rydberg level shifts, Δ_l, follow

$$\Delta_l = -\frac{E_0^2}{4}\,\alpha_0(\omega_{RF}), \tag{1}$$

where $\alpha_0(\omega_{RF})$ is known as the dynamic scalar polarizability in the SI units of MHz/(V/m)^2. The dynamic scalar polarizability is calculated from the electric-dipole matrix elements [28] and the frequency detuning of the RF from the atomic transitions of the Rydberg atom [7, 10]. The electric-dipole matrix elements and frequency detuning

have dependencies on fundamental constants that are SI-traceable to Planck's constant [29]. The polarizabilities typically scale as n^7 [6], where n is the principal quantum number of the atomic state. The fast scaling in n renders Rydberg atoms as ultrasensitive detectors for RF fields. Sample experimental EIT spectra of the $70S_{1/2}$ Rydberg-EIT line without and with incident RF fields are shown in Figure 1(A), demonstrating that an applied RF field at 2.5 GHz induces a red-shift (about 30 MHz in the case shown). The calculated quadratic behavior of the AC shift of the $70S_{1/2}$ level at an RF frequency of 2.5 GHz is plotted in Figure 1(B).

A major benefit of field detection in a regime where Eq. (1) is applicable is the low variation of α_0 over a frequency band ranging from DC to several GHz. This is shown in Figure 2(A) for the $nS_{1/2}$-states of ^{133}Cs. We display the scaled polarizability, $\tilde{\alpha}_0 = \alpha_0 \times ((n-\delta_s)/(90-\delta_s))^{6.72304}$, where the fast scaling of α_0 with n is divided out, and where we use the quantum defect of Cs S-type Rydberg states, $\delta_s = 4.049$ [6]. The scaling is necessary to arrive at a meaningful plot. In Figure 2(B), we show the frequency dependence of the (not scaled) polarizability α_0 for $70S_{1/2}$, as well as its deviation from the DC value, in percentage. We see that under the operating conditions used it is $\alpha_0(2\pi \times 2.5\,\text{GHz}) = 0.0648\,\text{MHz}\,(\text{V/m})^2$, and that α_0 varies by 4.4% over the range 2.2–2.8 GHz. We also note that $\alpha_0(\omega_{RF})$ can be calculated to a precision that does not affect the uncertainty of E_0. We choose the $70S_{1/2}$ Rydberg state for this work because it is at a principal quantum number n that provides a sensitive probe for RF fields at 2.5 GHz yet is low enough in n to be far from atomic resonances where there is significant variation in α_0, as shown in Figure 2(B).

The Rydberg state response to RF radiation deviates from Eq. (1) at stronger field amplitudes via Bloch–Siegert shifts and multiphoton processes, making the AC Stark shift model inaccurate [7, 30]. In this regime, a model based on Floquet theory [30] is required to obtain accurate field measurements, which we previously introduced to the field of Rydberg-based RF metrology [16, 11]. From Floquet theory, the solid curve in Figure 1(B) models the relationship between the detected 2.5 GHz RF field and the line shift Δ_l for the Cs Rydberg state $70S_{1/2}$. The Floquet result shows for $70S_{1/2}$ that higher-order shifts become noticeable for fields above ≈80 V/m, where the AC shift begins to deviate from the initially quadratic dependence on field predicted by Eq. (1). The maximum deviation of the approximate quadratic shifts obtained from Eq. (1) relative to the exact Floquet level shifts is seen in Figure 1(B), where near $E_0 = 100$ V/m the deviation reaches 5.0%. At higher values of n, where 2.5 GHz radiation is closer to atomic resonances and the atom-field coupling is generally stronger due to the larger atom size, the deviation of 5% occurs at lower field values. For instance, at $90S_{1/2}$, the models differ by 5% at $E_0 = 4.5$ V/m, whereas at $45S_{1/2}$, the 5% deviation does not occur until the field strength reaches 780 V/m. In the present RF measurement application, we implement Floquet level shifts (solid curve in Figure 1(B)) to convert measured AC shifts Δ_l into RF field amplitudes E_0.

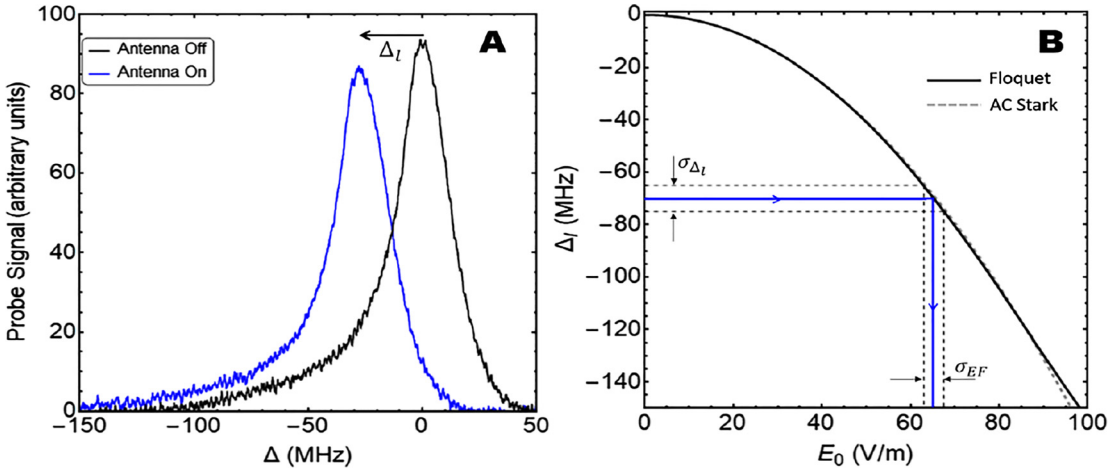

Figure 1: (A) Sample EIT spectra of the Cs Rydberg state $70S_{1/2}$ acquired with the RFP located near an antenna transmitter without an applied field (black) and with an applied 2.5 GHz RF field (blue curve). The data show an RF field–induced AC shift Δ_l of about 30 MHz. (B) Calculated AC shift Δ_l of the same state using Eq. (1) with $\alpha_0(2\pi \times 2.5\,\text{GHz}) = 0.0648\,\text{MHz}/(\text{V/m})^2$ (dashed) and using Floquet theory (solid curve) for a 2.5 GHz microwave field. In the field determination method employed in the RFMS, an AC shift Δ_l and its uncertainty σ_{Δ_l} are measured and converted to RF electric fields E_0 with uncertainties σ_{EF} using the Floquet calculation (blue arrows).

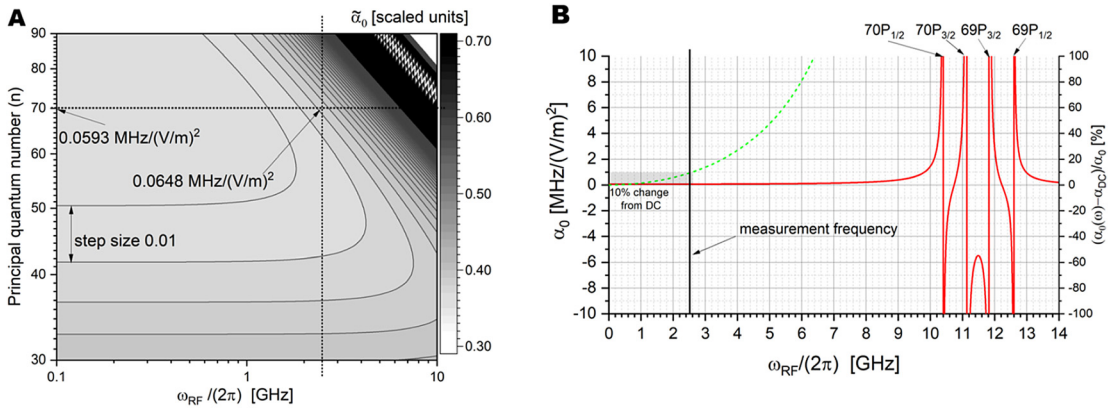

Figure 2: (A) Scaled scalar polarizability $\tilde{\alpha}_0$ for $nS_{1/2}$ Rydberg states of ^{133}Cs as a function of the RF field's angular frequency ω_{RF} and n. The spacing between the contour lines is 0.01, equivalent to ≈2.7% of the DC values of $\tilde{\alpha}_0$. We explicitly give the (not scaled) polarizabilities at $\omega_{RF} = 2\pi \times 2.5$ GHz and 100 MHz for $70S_{1/2}$, the Rydberg state used in Figures 1, 4, and 5. (B) $\alpha_0(\omega_{RF})$ for $70S_{1/2}$ (solid) and percentage change (dashed green curve) of $\alpha_0(\omega_{RF})$ relative to the *DC* value $\alpha_0(0)$, which is ≈9% at our operating point of 2.5 GHz (solid vertical line). The singularities are due to resonances at the transition frequencies from $70S_{1/2}$ to $70P_{1/2}$, $70P_{3/2}$, $69P_{3/2}$, and $69P_{1/2}$. The percentage change from DC is ≈9%at 2.5 GHz.

3 Experimental methods

We use the RFMS to measure and image the electric field of the near-field of a Yagi–Uda antenna using AC shifts of the Cs $70S_{1/2}$ Rydberg state. Yagi–Uda antennas are widely used to provide highly directional far-field patterns with a relatively small antenna profile compared with high-gain antenna dishes and other antenna structures. The Yagi–Uda antenna design makes use of induced currents on an array of parasitic elements [31, 32]. Typically, the linear array consists of parallel-wire ribs on a boom, with only one rib (feeder) being fed by an RF signal. The parasitic ribs often include a single reflector behind the feeder and a number of directors in front of the feeder. Usually, the feeder has a length smaller than 0.5λ, the reflector is slightly longer than the feeder, and the directors are somewhat shorter [1]. The spacing between the elements can range from 0.25 to 0.4λ with the reflector being closer to the feeder than the adjacent director [1]. This arrangement gives rise to an end-fire RF lobe pointing along the direction of the antenna boom in the far-field, providing typical directivities of ~10 dB for radiation in the UHF band. The Yagi–Uda design is a prime example of how complex wave interference can be harnessed to yield high directivity with a relatively small overall geometric footprint, presenting a suitable test case for measurements in a transmitter's near-field using a small RF probe. Figure 3 shows a simulation of the near-field radiation pattern of a Yagi–Uda antenna with element lengths and spacings for the DUT used in this study.

The measurement setup is illustrated in Figure 4(A). The RFMS is used with a portable Rydberg RF electric field probe (RFP), as described in the study by Anderson et al [23] and shown in Figure 4(B). The RFP consists of a Cs vapor-cell sensing element with a 10 mm diameter and length and counterpropagating 852 and 510 nm laser beams. During RF measurements, the 852 nm probe laser is frequency stabilized to the ^{133}Cs $F = 4$ to $F' = 5$ hyperfine transition on the D2 line and detected, while the 510 nm coupler laser scans through the resonance of the $6P_{3/2}$ to $70S_{1/2}$ transition for the spectroscopic EIT readout. For each spectrum, the relative frequency axis is provided by an optical frequency tracker and its absolute frequency obtained from a reference RF-field-free EIT spectrum for accurate field determination [23]. A Tupavco TP513 Yagi–Uda antenna is chosen as our DUT and is connected to an RF transmission line for emission at 2.5 GHz. The transmitter and RFP are both mounted at a distance of 0.753(5) m above a grounded plane. The RFP is translated in steps of 0.102 ± 0.005 m both parallel and perpendicular to the axis of the transmitting antenna. For each grid point, we simultaneously acquire an RF-induced AC-shifted EIT spectrum from the RFP and an RF field–free spectrum to which the shift in the RFP spectrum is referenced. Figure 1 illustrates the AC shift–based electric field determination method. Here, the peak position in the RFP spectrum is determined relative to that of the field-free spectrum to obtain the RF-induced shift Δ_l. The apparent asymmetry in the EIT spectra, attributed in part to perturbations of the Rydberg state within the vapor cell, does not impact the RF

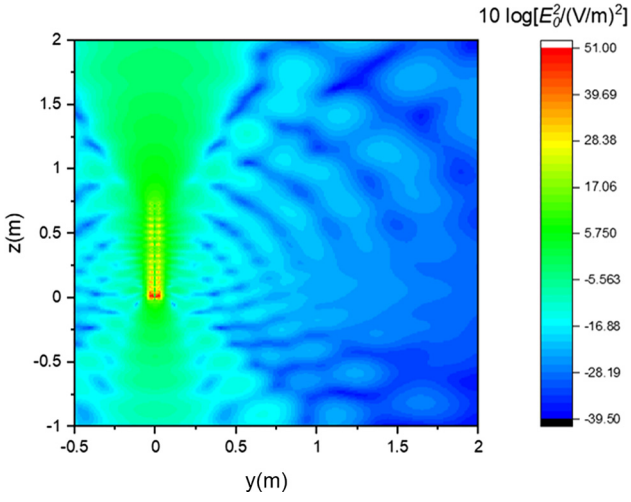

Figure 3: Simulation of near-field radiation pattern for a Yagi–Uda antenna with element length and spacing dimensions matching the DUT for a 1 V (10 mW) 2.5 GHz RF signal fed to the antenna. The antenna here is placed 0.753 m above an infinite ground plane.

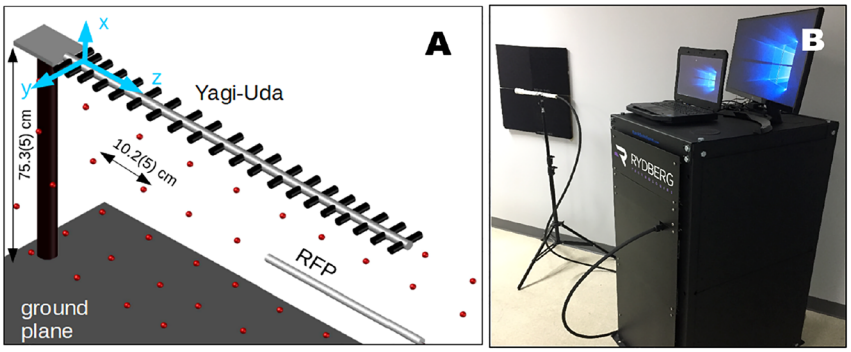

Figure 4: (A) An illustration of the measurement setup showing the orientation of the RFP with respect to the antenna DUT and ground plane. (B) The RFMS device with RFP used in this work.

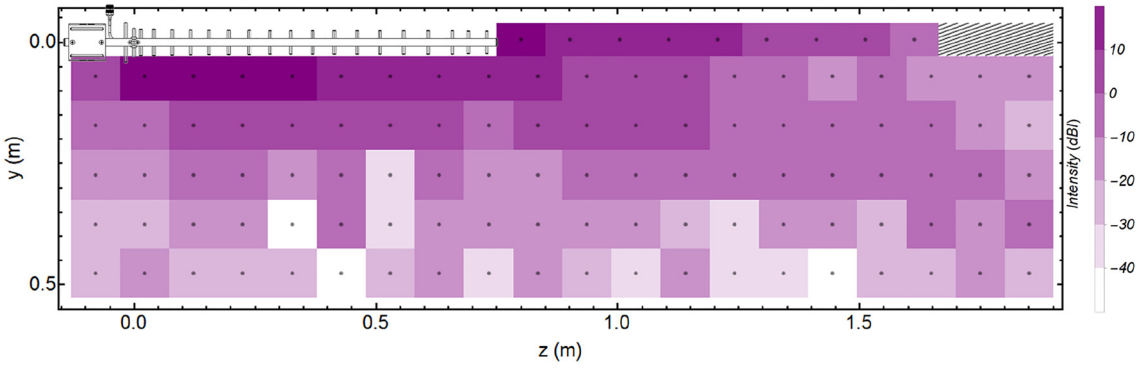

Figure 5: Map of the radiation pattern for the transmitting Yagi–Uda antenna. Each gray dot represents the actual position of the RFP during measurement, with step size $\Delta_y = \Delta_z = 0.102 \pm 0.005$ m. Measured electric fields or RF intensities are plotted in dBI as described in Eq. (2).

electric field determination because the asymmetry is static and independent of RF intensity. A discussion on the effect of asymmetric line shapes in SI-traceable RF electric field measurements and measurement uncertainties using Rydberg-based probes is provided in Ref. [23].

4 Measurement results

Figure 5 shows a composite image of the 2D electric field distribution measured by the RFP rastered over a 1.9×0.5 m area in the near-field of the Yagi–Uda antenna. The rastering grid covers half of the near-field plane which is symmetric about the antenna axis. At each RFP position on the grid, the electric field is derived from the RF-induced shift of the $70S_{1/2}$ Rydberg level relative to that of the field-free spectrum. From the shift, the precalculated Δ_f-versus-E_0 Floquet curve shown in Figure 1(B) is used to obtain the RF electric field amplitude E_0. Thus, the results of our detection yield an SI-traceable electric field amplitude measurement at each grid position in the near-field of the transmitting antenna and the resulting image shown in Figure 5. Here, the RF field strength is plotted in units of dBI[1] [11], where

$$\mathrm{dBI} = 10 \log \left[\frac{1}{2} c \epsilon_0 E_0^2 \big/ (\mathrm{W/m^2}) \right]. \tag{2}$$

In Figure 5 it is seen that even in the near-field most of the field is concentrated along the boresight of the antenna along z, with an apparent lobe along directions $\lesssim 15°$ from the z-axis. One also observes a general rapid drop-off in field strength as a function of distance from the antenna, as expected for the near-field. The wide dynamic range of ~40 dB in the measurements performed here with the RFMS is largely afforded by the implementation of AC Stark shifts. This enables continuous RF field measurement and imaging of the near-field behavior over a large spatial area and up to close proximity to the antenna transmitter.

1 Not to be confused with dBi, which represents the antenna gain relative to an isotropic emitter.

In Figure 6(A) we plot the measured field strength as a function of RFP position along the antenna boresight of the transmitting antenna. The field data in Figure 6(A) is fit to a function $A/(z-z_0)^3$ to obtain the expected position dependence of E_0 in the near-field of the Yagi–Uda antenna, which yields an effective center of the antenna charge distribution, z_0, and an amplitude A, which is proportional to the effective dipole moment of the DUT. Such a position dependence is expected as one approaches the near-field because of the multipole moments of the antenna's charge distribution that substantially contribute to the total radiating field. Here, our fit yields $z_0 = -0.710$ m and $A = 202$ Vm^2. In the near-field region, where $R < 2D^2/\lambda_{RF}$ [1], with D denoting the largest dimension of the antenna and R the distance from the DUT ($D \sim 80$ cm, the overall length of the array in our case), one would expect a significant contribution of the DUT's effective dipole moment on the field distribution and a $1/(z-z_0)^3$ dependence. In Figure 6(A), the data show good agreement with the dipole-like dependence on antenna position, which is represented by the solid, red curve. The data in Figure 6(A) and the fit residuals show that there are approximately periodic modulations in the field strength, with local maxima at $z = 1.03$ m, $z = 1.18$ m, and $z = 1.39$ m. We attribute these field-strength modulations mostly to interactions of the antenna and ground plane, which serves as a reflecting surface. This assumption is supported by simulations of the Yagi–Uda antenna modeled in Figure 3 placed 0.753 m above an infinite reflector, as shown in Figure 6(B) with a comparison with a simulation excluding the ground plane. In Figure 6(B), we display the simulated fields along the boresight of the antenna with and without the ground plane. Comparing Figure 6(A) and (B), it is seen that the simulated fields generally reproduce the measured field behavior very well. In addition, we find that the modulations in the field are in large part introduced by the grounded plane. Residual deviations of the field from a z^{-3} behavior, seen with the grounded plane removed, may arise from higher-order terms in the multipole expansion of the RF electric field, which are expected because of the large antenna size–to–wavelength ratio.

An uncertainties budget for the atomic RF measurement is provided in Table 1. Uncertainties resulting from the linearization of the 510 nm laser scan and statistical uncertainties from the local peak fits of the measured EIT spectra are included. Uncertainty resulting from standing RF waves inside the vapor cell is expected to be negligible due to the favorable ratio of the cell length ($D_{RFP} = 10$ mm) to RF wavelength ($\lambda_{RF} = 12$ cm), $D_{RFP}/\lambda_{RF} = 0.08$ [33], which has been separately quantified by simulations of the probe in its characterization. This characterization

Table 1: Relative uncertainty for each measurement point.

Uncertainty source	Relative uncertainty
Statistical (from local peak fits)	0.5%
Laser frequency linearity	0.3%
Positioning of RFP	5.5%

See text for details.

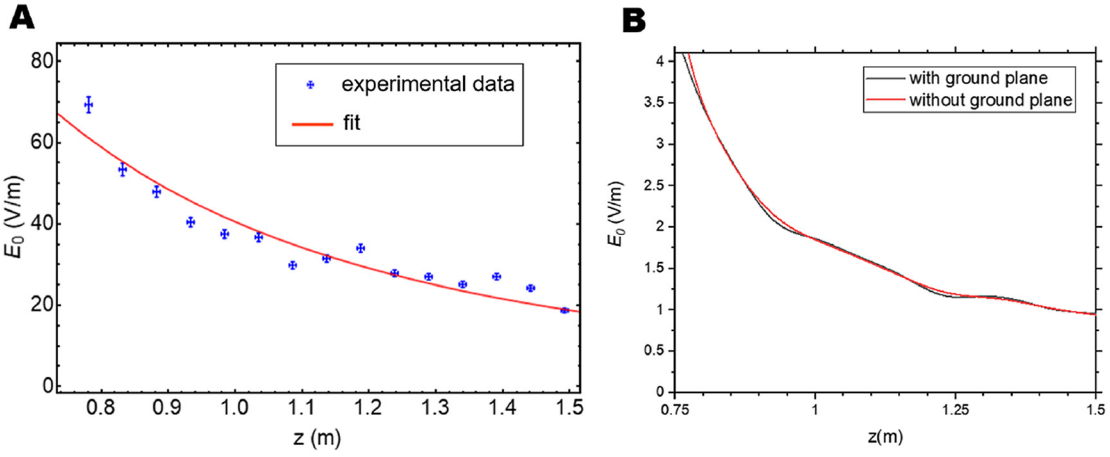

Figure 6: (A) RF electric field as measured by the RFP as a function of RFP position along the boresight axis of the Yagi–Uda antenna. The vertical error bars reflect the field-determination uncertainty arising from RFP position and alignment errors, and the horizontal error bars reflect RFP position uncertainty. The red line is a fit to the field data using the fit function $A/(z-z_0)^3$, with fit parameters A and z_0. (B) Simulation of the boresight axis for the Yagi–Uda model used in Figure 3. Here, the simulated antenna is fed 1 V of 2.5 GHz. The black curve is the simulation of the antenna spaced 0.753 m above an infinite ground plane; the red curve is the simulation of the antenna without the ground plane included.

and field inhomogeneities that also arise from the geometric orientation of the cell about the atomic-detection region are discussed in detail in the study by Anderson et al [23]. Simulations of the vapor cell immersed in a 2.5 GHz field based on a finite-element analysis provide a global probe calibration (C) factor of 0.8 [23]. This C factor means the free-space RF field amplitude is attenuated by 20% via the dielectric properties of the glass as it reaches the atomic-detection region. The uncertainties in our electric field measurements resulting from the positioning uncertainties of the RFP are determined empirically by measuring the RF field at grid position (0, 0, 1.08 m), which is near the center of the probed z-range along the antenna boresight, for different angular alignments of the RFP and for small position variations of the RFP. Specifically, the RFP position is varied in x and y by ±0.013 m, exceeding the experimental position uncertainty of 0.005 m. The RFP is also rotated by ±3° in the yz plane (this 3° probe-head rotation adds a linear translation of the sensor cell by 0.013 m). Finally, the RFP is rotated 360° about its own axis ϕ, in steps of 90°. The standard deviation and mean values of the field measurements are calculated, yielding an upper-bound to the relative measurement uncertainty due to positioning errors of the RFP of 5.5%. We add in quadrature all uncertainties from the sources listed in Table 1 and arrive at a total uncertainty of 5.5%, dominated by the RFP positioning uncertainty. This total uncertainty is represented by the vertical error bars in Figure 6(A). The atomic RF electric field measurement uncertainty from the atoms alone is below 1%.

5 Conclusion

In this work, we have demonstrated for the first time an atomic electric field measurement and imaging of a Yagi–Uda antenna near-field using a portable Rydberg atom–based field probe (RFP) and RFMS. The portable instrument is the first of its kind, which renders an all-optical spectroscopic readout of RF electric fields from a room-temperature atomic vapor in a subwavelength all-dielectric probe. The theory and application of off-resonant, RF-field level shifts in alkali Rydberg atoms is described and implemented in the probe for measurement of RF fields over a wide amplitude and frequency range, suitable implementation in atom-based RF metrology and testing and measurement applications with Rydberg atom–based detectors. A 2D image of the electric field distribution of the Yagi–Uda antenna near-field at 2.5 GHz was obtained and the field distribution along the antenna boresight was measured at subwavelength spatial resolution of $\lambda_{RF}/2$ with a measurement uncertainty of 5.5%, dominated by probe positioning uncertainty, and an atomic RF field measurement uncertainty below 1%. The expected leading dipole dependence in the near-field regime was measured.

Author contribution: All the authors have accepted responsibility for the entire content of this submitted manuscript and approved submission.
Research funding: This work was supported by Rydberg Technologies Inc. Part of the presented material is based upon work supported by the Defense Advanced Research Projects Agency (DARPA) and the Army Contracting Command-Aberdeen Proving Grounds (ACC-APG) under Contract Number W911NF-17-C-0007. The views, opinions and/or findings expressed are those of the author and should not be interpreted as representing the official views or policies of the Department of Defense or the U.S. Government.
Conflict of interest statement: The authors declare no conflicts of interest regarding this article.

References

[1] C. A. Balanis, *Antenna Theory: Analysis and Design*, Hoboken, New Jersey, John Wiley & Sons, Inc., 2016.
[2] W. L. Stutzman and G. A. Thiele, *Antenna Theory and Design*, 3rd ed., Hoboken, New Jersey, John Wiley & Sons, Inc., 2012.
[3] J. D. Jackson, *Classical Electrodynamics*, 3rd ed., Hoboken, New Jersey, John Wiley & Sons, Inc., 1999.
[4] D. Hill, M. Kanda, E. Laren, G. Koepke, and R. Orr, "Generating Standard Reference Electromagnetic Fields in the NIST Anechoic Chamber, 0.2 to 40 GHz," NIST Technical Note 1335, 1990. https://doi.org/10.6028/NIST.TN.1335 31.
[5] C. M. Schmid, S. Schuster, R. Feger, and A. Stelzer, "On the effects of calibration errors and mutual coupling on the beam pattern of an antenna array," *IEEE Trans. Antenn. Propag.*, vol. 61, p. 4063, 2013.
[6] T. F. Gallagher, *Rydberg Atoms*, Cambridge, England, Cambridge University Press, 1994.
[7] P. R. Berman and V. S. Malinovsky, *Principles of Laser Spectroscopy and Quantum Optics*, Princeton, New Jersey, Princeton University Press, 2011.
[8] K.-J. Boller, A. Imamoğlu, and S. Harris, "Observation of electromagnetically induced transparency," *Phys. Rev. Lett.*, vol. 66, p. 2593, 1991.
[9] J. Gea-Banacloche, Y.-Q. Li, S.-Z. Jin, and M. Xiao, "Electromagnetically induced transparency in ladder-type inhomogeneously broadened media: theory and experiment," *Phys. Rev. A*, vol. 51, p. 576, 1995.
[10] G. A. Costanzo, S. Micalizio, A. Godone, J. C. Camparo, and F. Levi, "ac Stark shift measurements of the clock transition in cold Cs atoms: Scalar and tensor light shifts of the D_{2} transition," *Phys. Rev. A*, vol. 93, 2016, Art no. 063404.
[11] D. A. Anderson, S. A. Miller, G. Raithel, J. A. Gordon, M. L. Butler, and C. L. Holloway, "Optical measurements of strong microwave

fields with Rydberg atoms in a vapor cell," *Phys. Rev. App.*, vol. 5, 2016, Art no. 034003.
[12] D. A. Anderson, G. Raithel, T. Nithiwadee, S. A. Miller, and A. Schwarzkopf, "Atom-based electromagnetic radiation electric-field and power sensor," 2018. US Patent 9,970,973 B2.
[13] A. K. Mohapatra, T. R. Jackson, and C. S. Adams, "Coherent optical detection of highly excited Rydberg states using electromagnetically induced transparency," *Phys. Rev. Lett.*, vol. 98, 2007, Art no. 113003.
[14] J. A. Sedlacek, A. Schwettmann, H. Kübler, R. Löw, T. Pfau, and J. P. Shaffer, "Microwave electrometry with Rydberg atoms in a vapour cell using bright atomic resonances," *Nat. Phys.*, vol. 8, p. 819, 2012.
[15] J. A. Gordon, C. L. Holloway, A. Schwarzkopf, et al, "Millimeter wave detection via Autler-Townes splitting in rubidium Rydberg atoms," *Appl. Phys. Lett.*, vol. 105, 2014, Art no. 024104.
[16] S. A. Miller, D. A. Anderson, and G. Raithel, "Radio-frequency-modulated Rydberg states in a vapor cell," *New J. Phys.*, vol. 18, 2016, Art no. 053017.
[17] D. H. Meyer, Z. A. Castillo, K. C. Cox, and P. D. Kunz, "Assessment of Rydberg atoms for wideband electric field sensing," *J. Phys. B.*, vol. 53, 2020, Art no. 034001.
[18] D. A. Anderson, R. E. Sapiro, and G. Raithel, "Rydberg atoms for radio-frequency communications and sensing: atomic receivers for pulsed RF field and phase detection," *IEEE Aero*, vol. 35, p. 48, 2020.
[19] D. A. Anderson, E. Paradis, G. Raithel, R. E. Sapiro, and C. L. Holloway, "High-resolution antenna near-field imaging and sub-THz measurements with a small atomic vapor-cell sensing element," in *2018 11th Global Symposium on Millimeter Waves (GSMM)*, 2018, pp. 1–3.
[20] H.-S. Lui, H. T. Hui, and M. S. Leong, "A note on the mutual-coupling problems in transmitting and receiving antenna arrays," *IEEE Antenn. Propag. Mag.*, vol. 51, p. 171, 2009.
[21] A. Yaghjian, "An overview of near-field antenna measurements," *IEEE Trans. Antenn. Propag.*, vol. 34, p. 30, 1986.
[22] F. Ferrara, C. Gennarelli, and R. Guerriero, "Near-field antenna measurement techniques," in *Handbook of Antenna Technologies*, Z. N. Chen, D. Liu, H. Nakano, X. Qing, and T. Zwick, Eds., Singapore, Springer Singapore, 2016, pp. 2107–2163.
[23] D. A. Anderson, R. E. Sapiro, and G. Raithel, "A self-calibrating SI-traceable broadband Rydberg atom-based radio-frequency electric field probe and measurement instrument," arXiv:1910.07107v2, 2019.
[24] Q. Gao, S. Liverman, and A. X. Wang, "Design and characterization of high efficiency nanoantenna couplers with plasmonic integrated circuit," *J. Lightwave Technol.*, vol. 35, p. 3182, 2017.
[25] Y. Xiang, S. Amarie, W. Cai, et al, "Real-space mapping of mid-infrared near-field of Yagi–Uda antenna in the emission mode," *Opt. Express*, vol. 27, p. 5884, 2019.
[26] J. Dyson, "Measurement of near fields of antennas and scatterers," *IEEE Trans. Antenn. Propag.*, vol. 21, p. 446, 1973.
[27] D. A. Steck, *Cesium D Line Data*, 2003, https://steck.us/alkalidata/.
[28] A. Reinhard, T. C. Liebisch, B. Knuffman, and G. Raithel, *Phys. Rev.* A, vol. 75, 2007, https://doi.org/10.1103/physreva.75.039902.
[29] B. Wood and H. Bettin, "The Planck constant for the definition and realization of the kilogram," *Ann. Phys.*, vol. 531, 2019, Art no. 1800308.
[30] S. Yoshida, C. O. Reinhold, J. Burgdörfer, S. Ye, and F. B. Dunning *Phys. Rev.* A, vol. 86, 2012, Art no. 043415.
[31] S. Uda, "On the wireless beam of short electric waves," *J. IEE (Japan)*, p. 273, 1926, https://doi.org/10.11526/ieejjournal1888.46.273.
[32] H. Yagi, "Beam transmission of ultra short waves," *Proc. IRE*, vol. 26, 715, 1928.
[33] H. Fan, S. Kumar, J. Sheng, J. Shaffer, C. Holloway, and J. Gordon, "Effect of vapor-cell geometry on Rydberg-atom-based measurements of radio-frequency electric fields," *Phys. Rev. Appl.*, vol. 4, 2015, Art no. 044015.